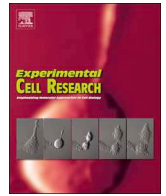




ELSEVIER

Contents lists available at ScienceDirect

Experimental Cell Research

journal homepage: www.elsevier.com/locate/yexcr

The actomyosin network is influenced by NMHC IIA and regulated by Crp^{F46}, which is involved in controlling cell migration

Yang Cao^{a,b}, Yan Lei^{a,b}, Yang Luo^a, Tan Tan^c, Baochen Du^a, Yanbo Zheng^d, Le Sun^e,
Qianjin Liang^{a,b,*}

^a Beijing Key Laboratory of Gene Resource and Molecular Development, College of Life Sciences, Beijing Normal University, Beijing 100875, PR China

^b Key Laboratory of Cell Proliferation and Regulation Biology of Ministry of Education, College of Life Sciences, Beijing Normal University, Beijing 100875, PR China

^c School of Pharmacology and Biology, University of South China, Hunan Province Cooperative innovation Center for Molecular Target New Drug Study, Hengyang 421001, PR China

^d The Institute of Medical Biotechnology (IMB) of the Chinese Academy of Medical Sciences, Beijing 100050, PR China

^e AbMax Biotechnology Co., Beijing 101111, PR China

ARTICLE INFO

Keywords:

Crp^{F46}
Cell migration
NMHC IIA
Centrosome
Stress fibers

ABSTRACT

When a cell migrates, the centrosome positions between the nucleus and the leading edge of migration via the microtubule system. The protein Crp^{F46} (centrosome-related protein F46) has a known role during mitosis and centrosome duplication. However, how Crp^{F46} efficiently regulates centrosome-related cell migration is unclear. Here, we report that knockdown of Crp^{F46} resulted in the disruption of microtubule arrangement, with impaired centrosomal reorientation, and slowed down cell migration. In cells that express low levels of Crp^{F46}, stress fibers were weakened, which could be rescued by recovering Flag-Crp^{F46}. We also found that Crp^{F46} interacted with non-muscle myosin high chain IIA (NMHC IIA) and that its three coiled-coil domains are pivotal for its binding to NMHC IIA. Additionally, analyses of phosphorylation of NMHC IIA and RLC (regulatory light chain) demonstrated that Crp^{F46} was associated with myosin IIA during filament formation. Indirect immunofluorescence images indicated that NMHC IIA filaments were inhibited when Crp^{F46} was under-expressed. Thus, Crp^{F46} regulates cell migration by centrosomal reorientation and altering the function of the actomyosin network by controlling specific phosphorylation of myosin.

1. Introduction

The centrosome is a non-membranous organelle in the cells of animals and some lower plants that acts as the microtubule-organizing center (MTOC); it not only serves as the kernel for nucleating microtubules (MTs) to assemble the spindle during mitosis [1] but also functions in maintaining cell morphology [2] and regulating cell migration [3]. When a cell migrates, it forms a pseudopodial protrusion and establishes polarity. With the exception of specific cells such as leukocytes and long-nosed potoroo (*Potorous tridactylus*) kidney (Ptk) cells [4–6], the centrosome is located between the nucleus and leading edge of migration in most types of animal cells [7–9] and is involved in the process of reorganizing the microtubule cytoskeleton to regulate cellular polarization [10,11]. The orientation of the nuclear centrosomal (NC) axis relative to the anteroposterior axis is a hallmark of cell polarity in the migrating cell, which is important for MT-based

vesicular trafficking (during transport by the Golgi apparatus) and nuclear migration. In particular, the highly conserved cell polarity complex composed of Par6 α and protein kinase C ζ (PKC ζ) [12] regulates myosin II, which participates in nuclear migration by virtue of its contraction, thereby enabling the nucleus to closely follow the centrosome during cell migration [13].

In living cells, the function of the cytoskeletal system depends on the coordination of MTs and actomyosin-regulated microfilaments [14]. Myosins comprise a large superfamily of molecular motors, of which there are at least 25 different classes [15]. These motors provide continuous contractile strength for the formation of the cleavage furrow in mitosis [16] and control cell migration and cellular morphology during interphase [17]. Non-muscle myosin II (NM II), one of the major types of myosin, consists of hexamers formed by two heavy chains (NMHC IIs), two regulatory light chains (RLCs) and two essential light chains (ELCs) [15,18]. Each NMHC is composed of three main parts: an N-

* Correspondence to: Beijing Key Laboratory of Gene Resource and Molecular Development, College of Life Sciences, Beijing Normal University, No. 19, XinJieKouWai St., HaiDian District, Beijing 100875, PR China.

E-mail address: lqj@bnu.edu.cn (Q. Liang).

<https://doi.org/10.1016/j.yexcr.2018.10.004>

Received 28 January 2018; Received in revised form 8 October 2018; Accepted 9 October 2018

Available online 15 October 2018

0014-4827/ © 2018 Elsevier Inc. All rights reserved.

terminal globular head with Mg^{2+} -ATPase catalytic activity that generates force, a light-chain binding domain, and an α -helical coiled-coil lever arm domain at the C-terminus that is responsible for dimerizing with another NMHC unit [19].

In mammalian cells, there are three isoforms of NMHC II (NMHC IIA, NMHC IIB and NMHC IIC), encoded by three different genes (*myh9*, *myh10* and *myh14*, respectively) [15,17]. Although these isoforms are homologous, they are differentially expressed in various tissues and differentially localized in cells, which demonstrates that they control various physiological processes. For example, NM IIA is involved in focal adhesion and the organization of stress fibers, which depends on the small GTPase Rho, whereas NM IIB is the functional unit for directing cell migration by coordinating protrusive activities and stabilizing cell polarity by affecting contraction of the ‘tail’ in cell migration [20]. Additionally, as an actomyosin-related enzyme, the function of myosin is regulated by phosphorylation at various sites within its NMHCs and RLCs. For example, phosphorylation of the RLC at Ser19 can greatly increase myosin activity [21] by controlling the conformation of the myosin heads, while phosphorylation of NMHC IIA at Ser1916 inhibits the aggregation of myosin rods into filaments, which disrupts the function of myosin [22].

Crp^{F46} (centrosome-related protein F46, GenBank accession: [KJ818093](#)) is a protein discovered by our group [23]. A previous study [23] showed that Crp^{F46} is a truncated variant of Golgin-245, and the identical polypeptide is in the C-terminal portion of Golgin-245, analyzed by the BLASTp method [23]. Crp^{F46} is located at centrosomes during interphase but is distributed throughout the cytoplasm during mitosis. It has three coiled-coil domains (CCI, CCII and CCIII), identified by SMART analysis. CCIII, which is relatively near to the C terminus, is the domain for Crp^{F46} to locate a centrosome. In addition, the reduction of its expression in HeLa cells inhibits cell growth and leads to abnormal cellular phenotypes, such as multiple nuclei, multiple centrosomes and multipolar spindles [23]. However, the molecular mechanism by which Crp^{F46} influences the physiological function of centrosomes and cell migration has not been clarified.

To further explore the function of Crp^{F46} and identify its co-operating partners, we used indirect immunofluorescence (IIF) to study Crp^{F46}-mediated regulation of centrosomal behavior and function in cells expressing low levels of Crp^{F46}. We found that normal intracellular Crp^{F46} level is necessary to maintain regular cell motility. When Crp^{F46} expression was decreased, cells migrating to wound displayed random centrosomal reorientation. We conducted a co-immunoprecipitation (Co-IP) assay and showed that NMHC IIA and Crp^{F46} interact directly. This interaction might help us understand the role of Crp^{F46} in cell migration regulation.

2. Materials and methods

2.1. Cell culture, reagents and antibodies

Cells were propagated in Dulbecco's Modified Eagle's Medium (DMEM) (Gibco, USA, 1645800) supplemented with 10% (v/v) fetal bovine serum (FBS) (Gibco, USA, 1231368) and penicillin/streptomycin (Solarbio, China, T1300) at 37 °C in a 5% CO₂ incubator. The reagents used in this study were DAPI (4', 6-diamidino-2-phenylindole) (Sigma, USA, D9542), blebbistatin (Cayman chemical, USA, 13165), rhodamine phalloidin (Cytoskeleton, USA, PHDR1), CT04 (Cytoskeleton, USA, # CT04). Mouse anti-His (D291-3), mouse anti-Flag (M185-3L), mouse anti-GAPDH (M171-3) and rabbit anti- α -tubulin antibodies (PM054) were produced by MBL, Japan. Rabbit anti-Cdc42 (2466T), rabbit anti-PKC ζ (9368S), rabbit anti-GM130 (12480T) antibodies were produced by CST, USA. Myosin light chain phosphor-regulation antibody sampler kit (MK6490) and myosin IIA heavy chain phosphor-regulation antibody sampler kit (MK6370) were produced by ECM biosciences, USA. The other antibodies used in our study were anti- γ -tubulin (Abcam, UK, ab179503), anti-NMHC IIA (Proteintech,

USA, 11128-1-AP), anti-Par6 (Bioss, China, bs-10350R). Second antibodies used in our study were alkaline phosphatase-conjugated goat anti-rabbit (7074P2) and goat anti-mouse (7076P2) IgG (CST, USA), and FITC/TRITC-conjugated goat anti-rabbit (111-095-003/111-025-003) and goat anti-mouse (115-095-003/112-025-003) IgG antibodies (Jackson, USA). The preparation of Crp^{F46}-specific polyclonal antibody was completed by both our laboratory (responsible for providing pure prokaryotic expression protein Crp^{F46} as antigens) and AbMax Biotechnology Company (China, responsible for immunization in mice). The oligonucleotides were synthesized by Shanghai Sangon Biotechnology, China.

2.2. Plasmid construction and transfection of cells

The Crp^{F46} deletion fragments S1 (amino acid residues 1–241), S2 (amino acid residues 127–426) and S3 (amino acid residues 323–530) were generated by PCR and cloned into the pET30a(+) prokaryotic expression vector (Novagen, USA, 69909) using the following primer pairs: 5' CGGAATTCGAAAGTTCACAGTCAGA 3' and 5' CCGCTCGAGT TTCTCCGTTCTGCCCGGC 3'; 5' CGGAATTCATACAGGCAAAGCAA ACT 3' and 5' CCGCTCGAGCAATTTCAATCACTGATTAA 3'; and 5' CGGAATTCATAAGGCCAGGAGGTGGAGG 3' and 5' CCGCTCGAGT CAAGATGAAGATCGGAG 3'. The pET30a(+)-Crp^{F46}-SP (splice fragment of Crp^{F46}) vector was synthesized by Biomed (China). The p3X-Flag-cmv-Crp^{F46} and pET30a(+)-Crp^{F46} expression vectors were constructed by PCR amplification of the pEGFP-C3-Crp^{F46} template with the following primers: 5' CCCAAGCTTATGGAAGTTCACAGTCAGAA ACAT 3 and 5' CGGGATCCAGATGAAGATCGGAGCCATGACAT 3'; and 5' GGAATTCGAAAGTTCACAGTCAGA 3' and 5' GGCTCGAGTCAAGA TGAAGATCGGAG 3', respectively.

The cells were transfected with Lipofectamine 2000 Reagent high-efficiency transfection reagent TransLipid (Invitrogen, USA, 11668-019H10129) according to the manufacturer's instructions. The transient transfections of cells were analyzed after 48 h being transfected. Alternatively, the cells were screened with 500 ng/ml G418 (Invitrogen, USA, 11811023) for 15 d, and stably transfected cell lines were established. Crp^{F46} low-expression HeLa cell lines used in this article were previously established [23].

2.3. Western blot (WB) analysis

For Western blot analyses, cell extracts or proteins expressed in *Escherichia coli* were denatured, separated by SDS-PAGE and transferred to a nitrocellulose membrane for 3 h with a 300 mA current; then, the non-specific proteins were blocked with 5% skim milk (Solarbio, China, 232100) in TBST (20 mM Tris-HCl, 150 mM NaCl, 0.05% Tween20) for 1 h at 37 °C. The antibodies were diluted with skim milk according to the manufacturers' protocols, and the membranes with the transferred polypeptides were probed. After three washes, the blots were incubated with peroxidase-conjugated secondary antibodies for 1 h at 37 °C and detected using an ECL (enhanced chemiluminescence) kit (Millipore, USA, WBKS0500) and Kodak BioMix films (Carestream, China, XBT).

2.4. Wound healing assays

The stably transfected cells were detached with trypsin, suspended in DMEM to a density of 2×10^5 cells per milliliter. The suspended cells were plated onto 96-well plates and cultured overnight to 90% confluence. Wounds were made until the sterile scaricator (IncuCyte Cell Migration Kit, Cat. No. 4493, USA) was put in the 96-well plates to slit the cellular monolayer and form wound about 0.8 cm in length and an average of 0.7 mm wide. The plates were washed with DMEM several times to remove the suspended cells. After replenishing with fresh medium without FBS, the dishes were placed in a 37 °C incubator with 5% CO₂ to drive cell migration. The cells in the wounded monolayers were imaged at the same positions every 1 h until wound healing with

IncuCyte live cell analysis system (Essen Bioscience, USA). The velocity of the migrating cells was measured using IncuCyte accompanying software with the following equation: $(1 - \text{wound area at the end time} / \text{wound area at the start time}) \times 100 (\%)$. The motion trails of signal cell were completed by Photoshop CS5 software.

2.5. Prokaryotic protein expression and pulldown assay

The recombinant pET30a(+) plasmids into which the entire coding sequences of Crp^{F46} or its deletion fragments S1, S2, S3 and SP were inserted were transformed into the BL21 bacterial strain (Biomed, China, BC201-01) to express the proteins. The prokaryotic His-tagged proteins were incubated with Ni²⁺ beads (GE, USA, 17-5268-01) for 1 h at 4 °C. The beads were washed three times with washing buffer (20 mM NaH₂PO₄, 0.5 M NaCl, and 80 mM imidazole, pH 7.4) at 4 °C. Then, the washed beads were incubated with the purified prokaryotic fusion proteins.

For the pulldown assays, the beads bound to the purified fusion proteins were incubated with lysates from HeLa cells over-expressing *Flag-Crp^{F46}* overnight at 4 °C. After isolation by centrifugation and washing, the bound proteins were eluted with SDS sample buffer and immunoblotted with anti-NMHC IIA and anti-His antibodies.

2.6. Indirect immunofluorescence, microscopy and image analysis

Cells were plated in 6-well tissue culture plates with coverslips and cultured to 90% confluence. Wounds were made by scraping with a pipette tip and were washed with DMEM several times to remove the suspended cells. Twelve hours after wounding, the coverslips were taken out.

The coverslips carrying cells were washed three times with PBS (pH 7.4). The cells were fixed with 4% paraformaldehyde at RT for 15 min, permeabilized with PBS containing 0.5% Triton X-100, washed, and then blocked with 5% skim milk in PBS for 1 h at 37 °C. The primary antibodies were diluted in PBST (PBS (pH 7.4) containing 0.1% Tween 20) according to the manufacturers' protocols and added to the cells, and the system was incubated overnight at 4 °C. After three more washes in PBST, the cells were incubated with FITC- or rhodamine-conjugated IgG (either anti-mouse or anti-rabbit) secondary antibodies diluted in PBST for 1 h at 37 °C. The cells were again washed three times with PBST and counterstained with DAPI. Images were acquired using a ZEISS Laser Scanning Confocal Microscope LSM700 (ZEISS, Germany) with a Plain-Apochromat 40 × /1.3 NA oil immersion lens. Images were analyzed using Zeiss Zen 2009 Light Edition software.

To quantify the disorder degree of microtubules and stress fibers arrangements, such as direction and density of filaments arrangement, we analyzed fluorescence images with Image J V1.5.1e software and utilized fractal dimension (D value). To quantify the degree of colocalization between Crp^{F46} and NMHC IIA, we analyzed confocal images using both Zen 2009 and Image-Pro Plus 6.0 softwares and utilized both Pearson's correlation coefficient (Rr) and a Manders' colocalization (R) analysis. For the methods for calculation of fractal dimension and coefficients (Rr and R), see the review by T.G. Smith, Jr [24] and Vadim Zinchuk [25].

2.7. Immunoprecipitation

The cells were harvested and solubilized with RIPA buffer (150 mM NaCl, 1 mM EDTA, 50 mM Tris, 0.25% sodium deoxycholate, and 1% NP-40, pH 7.5) containing protease inhibitors (0.1 mg/ml aprotinin and 0.1 mg/ml phenylmethylsulfonyl fluoride) for 30 min on ice. The samples were centrifuged at 13,000 × g for 20 min at 4 °C. The supernatant was incubated with Protein A/G Plus-Sepharose (TransGen Biotech, China, DP301-01) for 2 h at 4 °C and then incubated with antibodies overnight at 4 °C. After adding Protein A/G Plus-Sepharose, the mixture of protein extracts and beads was incubated for 4 h at 4 °C. After

centrifugation, the pellets were cleared and washed at least three times with RIPA buffer at 4 °C. The bound proteins were eluted with SDS sample buffer, centrifuged, and analyzed by Western blotting.

2.8. Myosin phosphatase inhibition and dephosphorylation assays

Cells were harvested and solubilized with extraction buffer (80 mM β-sodium glycerophosphate, 20 mM EGTA and 15 mM MgCl₂) containing protease inhibitors. After adding the phosphatase inhibitor cocktail (Biotool, USA, B14002) according to the manufacturer's protocols, the samples were centrifuged at 13,000 × g for 20 min at 4 °C following sonication. SDS sample buffer was added to the supernatant, and the proteins were denatured by boiling and analyzed by Western blotting.

For dephosphorylation assays, the cells were sonicated in extraction buffer with protease inhibitors on ice and centrifuged at 4 °C. The supernatant was mixed with lambda protein phosphatase (New England Biolabs, USA, P0753S) according to the manufacturer's protocols and incubated in a 37 °C water bath for 1 h. The dephosphorylation reaction was terminated with SDS sample buffer. Then, the samples were denatured by boiling and analyzed by Western blotting.

2.9. Statistical analysis

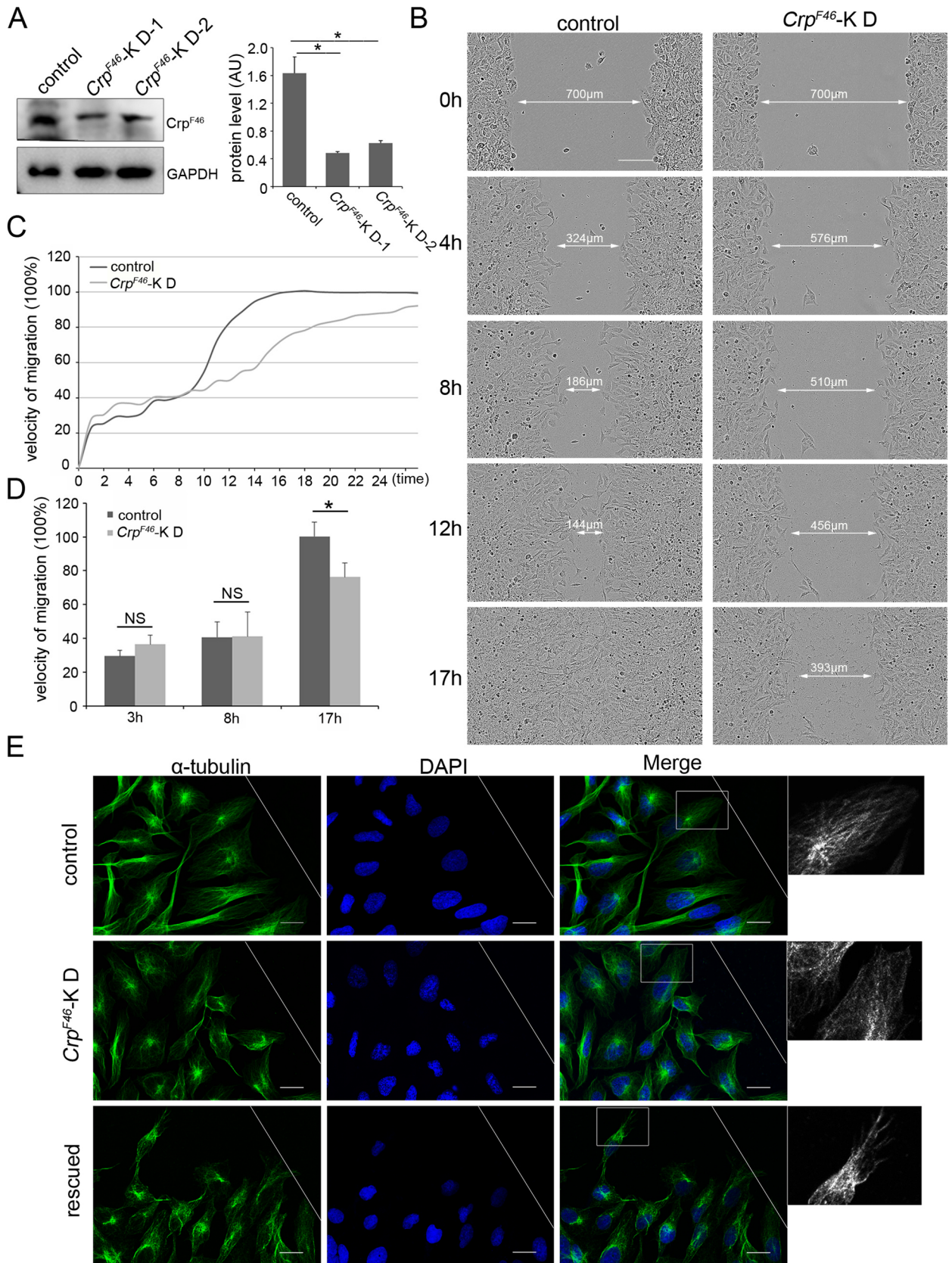
The experiments were repeated at least three times. The majority of the data are the averages or cumulative of several determinations. The statistical analyses were performed using the independent samples t-test solver tool in SPSS 16.0 software. The error bars showed the standard error of the mean ($\bar{X} \pm SE$). The P-values in the Figures are reported as *, $P < 0.05$; **, $P < 0.01$, and ***, $P < 0.001$.

3. Results

3.1. Knockdown of Crp^{F46} hinders cell migration by disrupting the arrangement of microtubules in cells

To test the influence of Crp^{F46} expression on cell migration, we chose human osteosarcoma cells, U-2OS, which possessed strong ability of movement and clear polarity, and obtained two stably transfected U-2OS cell lines, Crp^{F46}-knockdown-1 U-2OS and Crp^{F46}-knockdown-2 U-2OS cell lines, with the pXJ41 expression vector containing antisense RNA against Crp^{F46} (Fig. 1A). Crp^{F46}-knockdown-1 U-2OS cells were chosen to investigate the migration velocity using a wound healing assay, because of their higher Crp^{F46} depletion efficiency (around 70%) than that of Crp^{F46}-knockdown-2 U-2OS cells (around 60%) and their expression level of Golgin-245 is not different from that of the control cells in mRNA level (Supplementary material Fig. S1B). The wounds of the control cells (transfected with a pXJ41 vector without the antisense gene insert) required approximately 17 h to heal, whereas the wounds of the Crp^{F46}-knockdown cells were still open 17 h after wounding, displaying delayed cell migration (Fig. 1B). Analyzed with the IncuCyte live cell analysis system, the line chart (Fig. 1C) showed that, during the initial stage of migration, the velocity of Crp^{F46}-knockdown cell matched the velocity of control, and even in the first 3 h or 8 h, the velocity statistics of both cell lines was no significant difference ($P = 0.164$ and $P = 0.128$, respectively, Fig. 1D). Interestingly, however, when cells migrated 8 h later, compared with control cells, the velocity of Crp^{F46}-knockdown cells declined dramatically ($P = 0.036$, Fig. 1D) and ultimately failed to heal within 17 h (Fig. 1B and C). Meanwhile, we also performed wound healing assay with HeLa cells. Similarly, the differences in velocities were not statistically significant in the first 24 h after wounding. However, after 48 h or 60 h, the velocities were significantly lower than that in the control cells ($P < 0.01$) (Supplementary material Fig. S1D-F).

As previously reported [23], Crp^{F46} locates in the centrosome and influence the function of MTOC. Meanwhile, the basic role of MTOC is



(caption on next page)

Fig. 1. Reduced expression of Crp^{F46} in U-2OS cells decreases the rate of cell migration and disrupts the arrangement of microtubules (A) Left: Western blots with an anti- Crp^{F46} polyclonal antibody were used to analyze the transfection efficiency of pXJ41-antisense- Crp^{F46} into U-2OS cells. Right: Histogram showing relative protein level of the left image. (B) Confluent cultures of Crp^{F46} -knockdown U-2OS cells and control cells were wounded by scratching, and images were obtained with IncuCyte live cell analysis system and showed situations of wound every four hours until healing completely. The scale bar represents 150 μm . (C) Line graph showing the velocity of migration in the control and Crp^{F46} -knockdown cells. (D) The time-segmented migration velocities of the control and Crp^{F46} -knockdown cell are presented in a histogram. (E) U-2OS cells stably transfected with an empty vector, the pXJ41-antisense- Crp^{F46} vector or the pAcGFP1-Hyg-C1- Crp^{F46} vectors were scratched and observed with a ZEISS Laser Scanning Confocal Microscope LSM700 after 12 h. The visible microtubule network was stained with a polyclonal anti- α -tubulin antibody, and the cell nuclei were counterstained with DAPI. Microtubules of cells in boxes are displayed in black and white. Long white lines referred to the width of scratches (also in subsequent Figures). The scale bars represent 20 μm . The data in the bar graphs are presented as the mean \pm SD; * and ** represent $P < 0.05$ and $P < 0.01$, respectively (also in subsequent Figures).

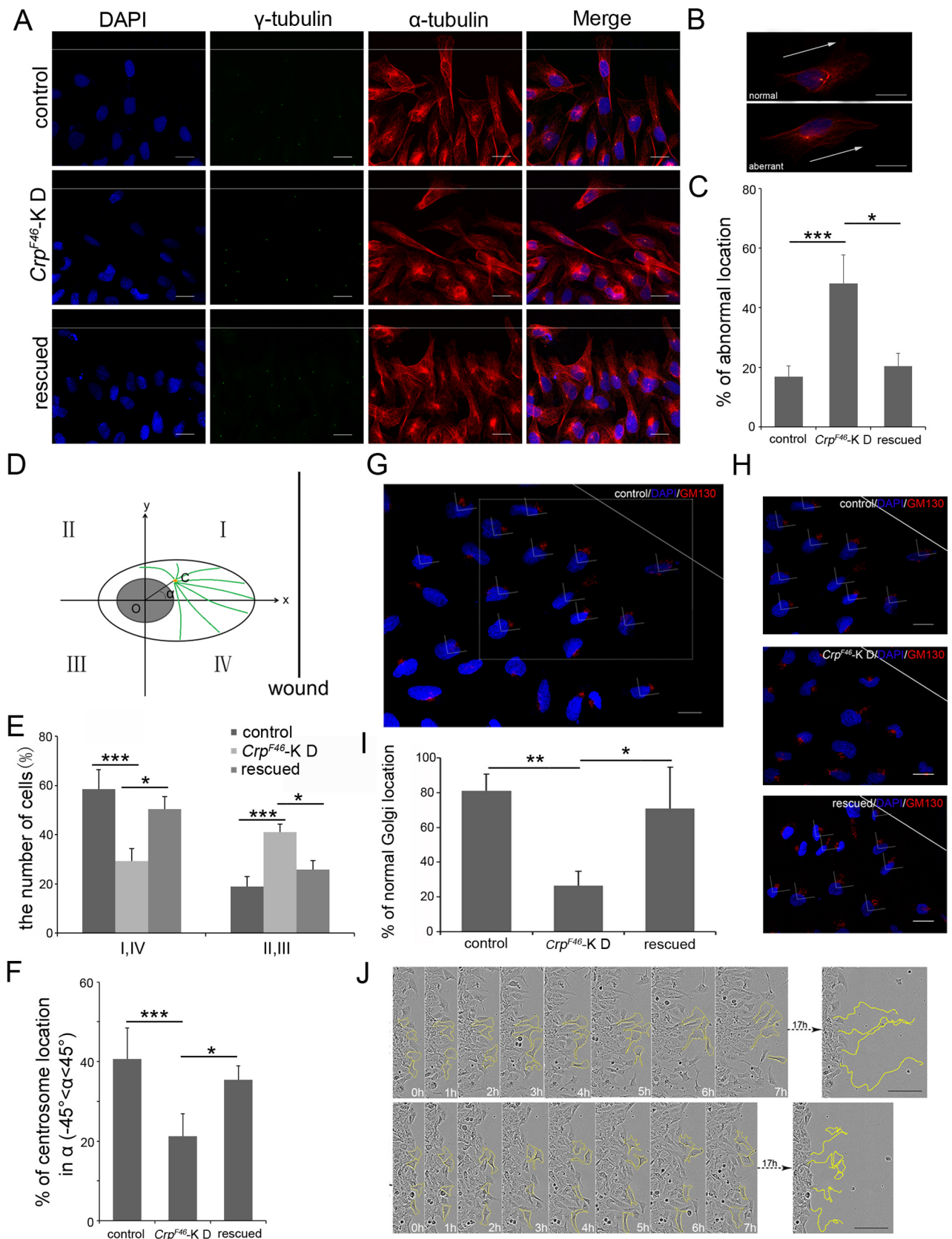
nucleating microtubules. To further explore whether the reduction in cell migration of the Crp^{F46} -knockdown cells is related to the assembly, structure or dynamic behavior of microtubules, we immunostained the cells and monitored cellular behavior by confocal microscopy (Fig. 1E). We observed that microtubules in the control cells were compacted and arranged in fascicular clusters facing the open area of the wound. However, the Crp^{F46} -knockdown cells at the wound margin displayed circular shapes. Their microtubule networks surrounding the nucleus were loose and disorganized. We also stably transfected recombinant pAcGFP1-Hyg-C1- Crp^{F46} vectors into Crp^{F46} -knockdown U-2OS cells to replenish the deletion of Crp^{F46} (Supplementary material Fig. S1G). The microtubules of rescued U-2OS cells was stained by α -tubulin antibody and was observed be neatly fascicular clusters, like control cells (Fig. 1E). To describe the microtubules arrangements (fascicular or loose and disorganized) objectively, we calculated the fractal dimension (D value) of both cell lines. Fractal dimension is a standard for evaluating cell process complexity. The higher D value represents the more complex situation, and vice versa [24,26]. The statistics of D value from 50 cells showed that the difference of complexity between control cells and Crp^{F46} -knockdown cells achieved high significant level ($D_{\text{control}} = 1.78 \pm 0.00031$, $D_{\text{Crp-K}}^{F46} = 1.83 \pm 0.00043$, $P = 0.0011$). The D value of cells treated 3 h by nocodazole, as a reference group, was 1.74 ± 0.0010 . For function of nocodazole, the tubulins were depolymerized and their arrangement became too simple to unclear, which led to D value reduce, comparing with control cells. Therefore, the D value of control and Crp^{F46} -knockdown cells showed the arrangement of microtubules in control cells were neater than it in Crp^{F46} -knockdown cells. The Similar phenotype in HeLa cell lines can also be found (Supplementary material Fig. S1H). These results suggested that reduced Crp^{F46} expression affects cell migration by the disruption of microtubules arrangement.

3.2. Knockdown of Crp^{F46} strongly affects centrosomal reorientation and cell polarity during cell migration

The centrosome, as the main center for microtubule organizing, is closely linked to microtubule dynamics, and its position forms the rear-front axis with the nucleus as the hallmark of cell polarization [27], which is pivotal for cellular directional movement and influences the velocity of migration significantly. Therefore, we monitored changes in microtubule and centrosome reorientation in the scrape-wound migration assay. The resulting confocal images showed that the relative positions of the centrosome, nucleus and wound edge were randomly oriented in the Crp^{F46} low-expressing U-2OS cells because they had lost their ability to undergo cell polarization (Fig. 2A). As shown in Fig. 2B, cell migration requires cell polarization, i.e., it requires the centrosome to be located between the nucleus and the leading edge of migration. We assessed the positions of the centrosomes in single moving cells which located in the front row, adjoining the scratch, and quantified the percentage of cells with abnormally located centrosomes. There was a highly significant difference between the results from the Crp^{F46} -knockdown cells and control cells ($P = 1.14 \times 10^{-5}$) (Fig. 2C). The rescued cells were also immunofluorescently stained and quantified according to the same measuring method of the control and Crp^{F46} -knockdown groups. The percentage of cells with abnormally located

centrosomes decreased, comparing with Crp^{F46} -knockdown cells (Fig. 2C). Next, we calculated the x and y rectangular coordinates for the peripheral cells, with the origin at the center of the nucleus and the x-axis representing the direction of cell migration (Fig. 2D). In order to test the rate of development of the cellular poles toward the wound edge, we calculated the percentage of cells that had centrosomes in quadrants I and IV or in quadrants II and III. There was a highly significant difference in the percentage of centrosomes located in quadrants II and III between the two cell lines (Crp^{F46} -knockdown and control cells) ($P < 0.001$), and a significant difference in quadrants I and IV between Crp^{F46} -knockdown cells and the rescued cells ($P = 0.0342$) (Fig. 2E). Furthermore, as shown in Fig. 2D, the center of the nucleus was marked as the origin (O), and the position of the centrosome was labeled C. By measuring the angle between the OC vector (pointing from O to C) and the positive direction on the x-axis, we demonstrated that the percentage of cells with angles between -45° and 45° was significantly different between the Crp^{F46} -knockdown U-2OS cells ($P = 3.09 \times 10^{-4}$) and control cells (Fig. 2F). The statistics of rescued cells indicated there was an increase in the percentage of cells with angles between -45° and 45° (Fig. 2F). The same measurements had been used to analyze two HeLa cell lines (control and Crp^{F46} -knockdown). The statistical data also displayed results similar to U-2OS cell lines (Supplementary material Fig. S2B-D).

Cell polarization is reflected in the centrosome location, and associated with that, it is also embodied by the location of Golgi apparatus (GA) in moving cells. To display cell polarity, labeling by Golgi maker protein, GM130, we can clearly see that the rule of the GA' location (facing wound) is more severe near the wound (Fig. 2G). We measured the cells adjoining the scratches and found, in cell polarity aspect, a high significant difference between control and Crp^{F46} -knockdown cells. Meanwhile, the energy of cell polarization was resumed with the rescue of Crp^{F46} (Fig. 2H and I). In corresponding detection, a high significant difference was also showed between two HeLa cell lines (Supplementary material Fig. S2F and G), though HeLa cells have poor ability of polarization. Cdc42, a small GTPase of Rho family, is famous for the key role in establishing cell polarity by promoting microtubule growth and inducing actin polymerization in cell directional migration [28,29]. Active Cdc42 recruits Par complex [30] which is composed of Par6 and PKC ζ and promotes microtubule-mediated centrosome reorientation [30,31]. We used Cdc42 and Par complex as makers to estimate the level of cell polarity of the two cell lines. The Western blot results showed that the protein level of Cdc42 reduced by half when Crp^{F46} was low-expressed, while Par6 and PKC ζ in two HeLa cell lines had no difference ($P = 0.853$ and $P = 0.534$, respectively, Supplementary material Fig. S2H and I). We also focused on the trajectory of single-cell migration, which is the most intuitive manner to observe cell polarity. Observed accurately with IncuCyte live cell analysis system, the control cells moved towards scratch directly; however, the movement trajectory of Crp^{F46} -knockdown cells was winding and non-directional, which was consistent with previous report [3] (Fig. 2J and Supplementary material Fig. S2E). All of these results indicated that the reduced Crp^{F46} expression seriously affected centrosomal reorientation and cellular polarization, which can lead to non-directional movement.



(caption on next page)

Fig. 2. Knockdown of Crp^{F46} strongly affects centrosome reorientation during cell migration (A) Confocal images of control cells, Crp^{F46} -knockdown U-2OS cells and rescued cells captured on a ZEISS Laser Scanning Confocal Microscope LSM700. The centrosomes and microtubules were labeled with an anti- γ -tubulin antibody (green) and anti- α -tubulin antibody (red), respectively, 12 h after the cell monolayers being scratched. Long white lines referred to the width of scratches. The scale bars represent 20 μ m. (B) The criterion used to evaluate the normal position of the organelles during cell migration is shown at the top. The centrosome (stained in green) was located between the leading edge of the cell (stained in red) and the cell nucleus (stained in blue). The image at the bottom shows the abnormal positions of the organelles during cell migration. Arrows represent the direction of cellular motion. The scale bars represent 20 μ m. (C) The results are shown in a histogram based on the evaluation criterion on the (B) ($n = 500$, $P = 1.14 \times 10^{-5}$ and $P = 0.0342$). (D-F) Diagrams illustrating the quantitative standards of centrosomal relocation. The nucleus of a cell located at the scratch edge was designated the origin, O. We established a rectangular coordinate system and defined the direction of cell motility as the x-axis (D). Histogram showing the percentage of centrosomes located in quadrants I and IV or quadrants II and III (E) ($n = 500$, quadrants I and IV: $P = 2.54 \times 10^{-5}$ and $P = 0.0389$, quadrants II and III: $P = 2.49 \times 10^{-5}$ and $P = 0.0433$). The position of the centrosome was defined as C and formed a vector OC with the origin of the coordinate system. The angles between OC and the x-axis are expressed in a bar chart (F) ($n = 500$, $P = 3.09 \times 10^{-4}$ and $P = 0.0228$). (G-H) Fluorescence images showed Golgi location in U-2OS cells. In panel G, the region in the dotted box refers to the observation of H. In control cells, Crp^{F46} -knockdown cells and rescued cells, the Golgi apparatuses and nuclei were labeled with anti-GM130 antibodies (red) and DAPI (blue), respectively. Angles by two white short lines refers to the area facing scratch. The scale bars represent 20 μ m. (I) Histogram showing the percentage of Golgi location facing scratch ($n = 500$, $P = 0.0018$ and $P = 0.0217$). (J) The Crp^{F46} -knockdown U-2OS cells and control cells were tracked every hour during migration. The images behind arrowhead showed the trajectories of migrating in 17 h. The yellow lines referred to traces of cell movement. Cells circled by yellow lines were points of focus. The scale bars represent 150 μ m.

3.3. Crp^{F46} interacts with non-muscle myosin heavy-chain IIA (NMHC IIA)

To explore the molecular mechanism by which Crp^{F46} affects cell migration, we transfected recombinant p3 \times Flag-cmv- Crp^{F46} vectors into HeLa cells (Fig. 3C) and performed Co-IP with anti-Flag antibodies. Analysis of the Protein A/G Plus Sepharose-bound proteins by SDS-PAGE and Coomassie brilliant blue staining revealed a clear band of approximately 220 kDa (Fig. 3A). After isolating the polypeptide band and sequencing it by tandem mass spectrometry (MS/MS), we tallied the results and discovered that the peptide sequence was identical to NMHC IIA (data not shown). To validate the MS/MS result, a Co-IP assay followed by Western blotting was performed and showed that Crp^{F46} bound to NMHC IIA in HeLa cells expressing Flag- Crp^{F46} (Fig. 3B). NMHC IIB is another isoform of non-muscle myosin heavy chain and has similar structure with NMHC IIA. Hence, we used NMHC IIB as a negative control. In addition, to assess the interaction between Crp^{F46} and NMHC IIA *in vitro*, we investigated the interaction with a pulldown assay, which clearly demonstrated that the *in vitro* expressed Crp^{F46} and endogenous NMHC IIA directly interacted (Fig. 3D). Moreover, we wanted to identify the specific part of Crp^{F46} that is essential for its interaction with NMHC IIA. Because the structure of Crp^{F46} contains three coiled-coil (CC) domains [23], we constructed recombinant vectors containing each of the four Crp^{F46} fragments, as shown in Fig. 3E. These vectors were used for pulldown assays. Interestingly, all the three CC domains of Crp^{F46} (corresponding to fragments S1–S3) were able to interact with NMHC IIA, but another Crp^{F46} fragment (SP), the inter-CC region fusion protein, failed to bind NMHC IIA (Fig. 3F). To remove the false positive results of the experiment, PCNA, a protein we had already identified to only interact with S1 fragment of Crp^{F46} (data not published), was used as the negative control for S2/S3 fragment to reconfirm the interactions between the CC fragments of Crp^{F46} and NMHC IIA.

As shown in the indirect immunofluorescence images (Fig. 3G), microfilaments labeled by rhodamine-phalloidin co-localized with NMHC IIA stained with Alexa Fluor 647-labeled polyclonal rabbit anti-NMHC IIA antibody. Interestingly, Crp^{F46} stained with anti- Crp^{F46} antibody co-localized with NMHC IIA as well to an extent, although it was localized to the centrosomes during interphase, while NMHC IIA was localized in the cytoplasm. The analysis of layer-by-layer scan also displayed the co-localization between Crp^{F46} and NMHC IIA (Fig. 3G). Additionally, this phenotype was quantified by using the Pearson correlation coefficient (Rr) and Manders' overlap coefficient (R). The Pearson correlation coefficient describes the correlation of the intensity distribution between the channels (e.g. red and green), where the values range from -1.0 to 1.0 and > 0.5 indicates significant correlation. The Manders' overlap coefficient indicates the actual overlap of the signals, where the values range from 0 to 1.0 and > 0.6 denotes significant correlation [25]. We selected Crp^{F46} fluorescence areas in 20

cells as ROI (region of interest) and measured Rr and R of these areas. The calculated Rr was 0.514 ± 0.09 and R was 0.873 ± 0.04 for Crp^{F46} and NMHC IIA. These results indicated that Crp^{F46} indeed co-localized with NMHC IIA. These data suggest that Crp^{F46} may function by interacting with NMHC IIA.

3.4. Crp^{F46} functions in the formation of the microfilament network regulated by NMHC IIA

Recent studies have shown that NM II reversibly binds to actin filaments [15] and regulates stress fiber formation during cell migration [14,32]. To identify the function of NM II, we respectively treated HeLa cells with two drugs inhibiting NM II activity. One is blebbistatin, which specifically inhibits the ATPase activity of myosin II; another one, CT04, is a Rho inhibitor which inactivates Rho kinase (ROCK) and stays function of NM II. After drug treatment, the HeLa cells displayed some similar phenotypic features, such as frail and dim stress fibers (Fig. 4A and B). We adopted fractal dimension analysis again to quantify the phenotypic of stress fibers. The D value of cells treated by blebbistatin was significantly below that of the control cells' ($D_{DMSO} = 1.73 \pm 0.0054$, $D_{BLB} = 1.58 \pm 0.0099$, $P = 2.98 \times 10^{-7}$). The D value of cells treated by CT04 reduced significantly as well ($P = 0.0036$). This corroborated that the activation of NMHC IIA may be a key factor in regulating the formation of the actomyosin network.

It is not difficult to understand that Crp^{F46} -NMHC IIA interaction reminds us a possible functionalist linkage between Crp^{F46} and microfilament. For this reason, we stained microfilaments with rhodamine-conjugated phalloidin (Fig. 4C), and discovered that, like cells treated by inhibitors, the stress fibers in the Crp^{F46} -knockdown HeLa cells adjoining wounds were weakened, even almost undetectable, while the stress fibers of control cells were clearly visible. The D value of Crp^{F46} -knockdown cells was significantly smaller than control cells' ($D_{control} = 1.73 \pm 0.009$, $D_{Crp-KD} = 1.68 \pm 0.0056$, $P = 0.043$). To ensure the anomaly of stress fibers due to lack of Crp^{F46} , we transiently transfected recombinant p3 \times Flag-cmv- Crp^{F46} vectors into Crp^{F46} -knockdown HeLa cells, and observed (Fig. 4D), in HeLa cells labeled by anti-Flag antibody, the stress fibers were rescued. These data indicated that Crp^{F46} guaranteed the formation of the microfilament network which is regulated by NM II.

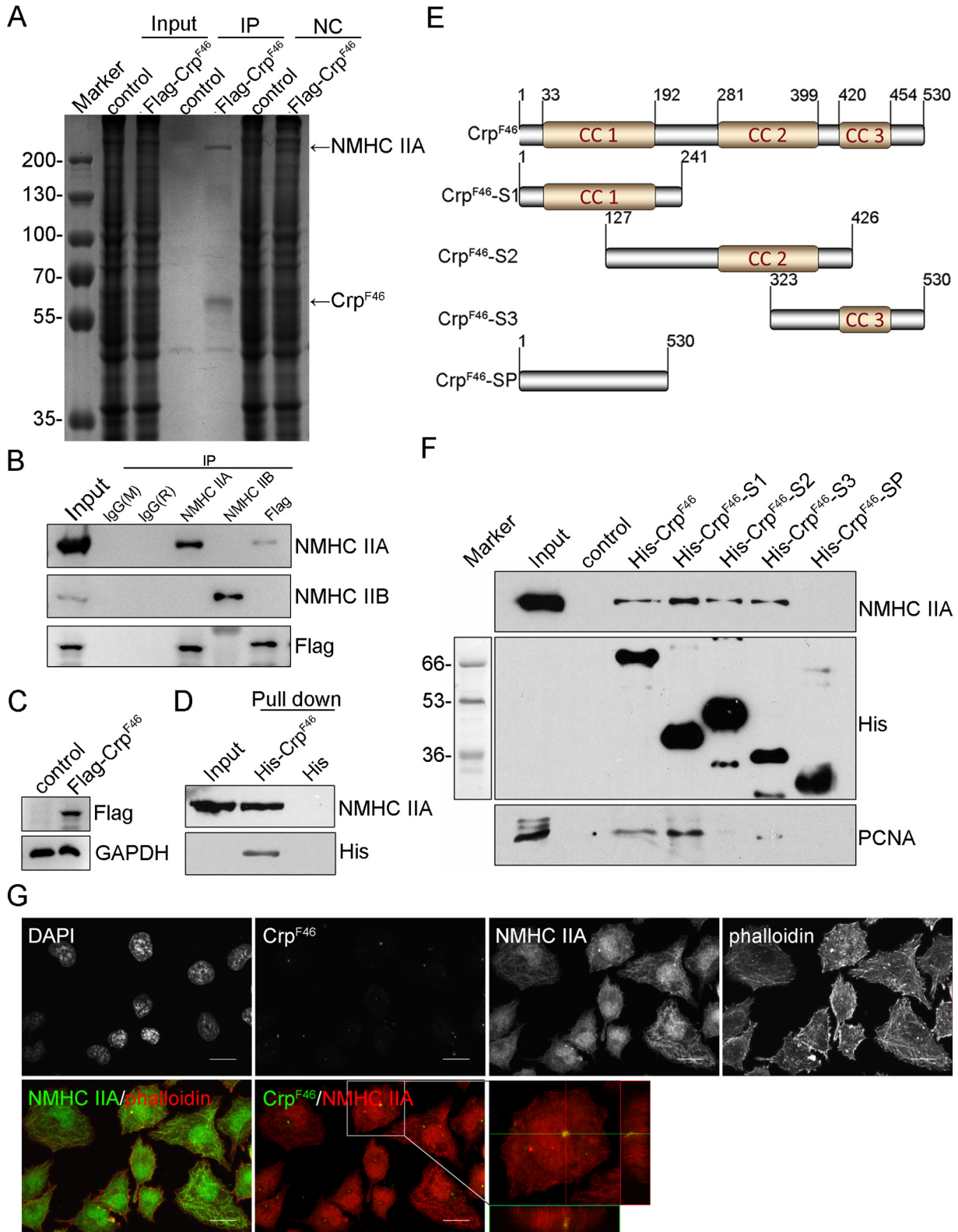
3.5. Crp^{F46} regulates the actomyosin network through phosphorylation of myosin and myosin filament formation

To identify the adjustment relationship between Crp^{F46} and NMHC IIA, a Western blot assay was performed, which showed that there was no significant difference in the expression of NMHC IIA between the Crp^{F46} -knockdown HeLa cells and control cells (Fig. 5A and B). It was illustrated that Crp^{F46} doesn't impact the function of NMHC IIA by

protein expression level. Therefore, we hypothesized that the reduced expression of *Crp^{F46}* blocks the activity of myosin IIA by disrupting the interaction between *Crp^{F46}* and NMHC IIA.

Phosphorylation is one of main posttranslational regulatory mechanisms of myosin activity, and occurs on the heavy chain and the associated regulatory light chain [33]. To identify the reason behind the

reduction in myosin activity, we performed a control experiment by treating proteins extracted from control cells and *Crp^{F46}*-knockdown HeLa cells with a phosphatase inhibitor cocktail and Lambda protein phosphatase. A series of Western blot assays with phosphorylation-specific antibodies against NMHC and RLC (Fig. 5C and D) showed that the level of NMHC IIA phosphorylation at Ser1916 and Ser1803



(caption on next page)

Fig. 3. Crp^{F46} interacts with non-muscle myosin heavy-chain IIA (NMHC IIA) (A) An immunoprecipitation (IP) assay was performed with an anti-Flag antibody, and the protein mixture extracted from the IP was separated on a 7% SDS-PAGE gel and stained with Coomassie brilliant blue (CBB) G250. Input: protein of whole control cells and Flag-Crp^{F46} cells; IP: protein binding with Protein A/G Plus-Sepharose; NC (negative control): protein of cells extract after binding with Protein A/G Plus-Sepharose (B) IP-Western blotting (IP-WB) was performed to analyze the IP products from the Flag-Crp^{F46}-expressing HeLa cells using an anti-Flag antibody, an anti-NMHC IIA antibody and an anti-NMHC IIB antibody. (C) Western blots with an anti-Flag antibody were used to analyze the transfection efficiency of p3×Flag-cmv-Crp^{F46} into HeLa cells. (D) Pulldown products of full-length Crp^{F46} purified from *E. coli* BL21 transformed with pET30a-Crp^{F46} were analyzed by Western blotting with an anti-His-tag antibody and anti-NMHC IIA antibody. (E) Diagram of the full-length Crp^{F46} amino acid sequence showing the locations of the three coiled-coil domains, CCI, CCII and CCIII, and the positions of the corresponding deletion fragments of Crp^{F46}, including fragments of Crp^{F46} containing only one coiled-coil domain (Crp^{F46}-S1, S2 and S3) and fragment of Crp^{F46} without any coiled-coil domain (Crp^{F46}-SP). (F) Western blotting analysis of the pulldown products from the HeLa cells and the prokaryotically expressed full-length Crp^{F46} protein and Crp^{F46} fragments. (G) Confocal microscopy gray pictures showed HeLa cells stained with a murine anti-Crp^{F46} polyclonal antibody, a rabbit anti-NMHC IIA polyclonal antibody and phalloidin. The color image on the left showed microfilaments (red) and NMHC IIA (green) were co-localized. The color image on the right showed that Crp^{F46} (green) and NMHC IIA (red) were co-localized. The cell circled in box was amplified which showed its fluorescent signal of cross and longitudinal section to its side. The colors in the images were false-colors. The scale bars represent 20 μm.

between Crp^{F46}-knockdown cells and control cells were all in very significant difference ($P = 5.42 \times 10^{-4}$ and $P = 7.61 \times 10^{-5}$, respectively). While the difference in phosphorylation levels at another phosphorylation site, Ser1943, on NMHC IIA was not distinct between the two cell lines ($P = 0.058$). However, compared with the control cells, the phosphorylation of Ser1 on RLC was increased highly significantly ($P = 1.58 \times 10^{-4}$), but the phosphorylation of Ser19 on RLC was reduced significantly ($P = 0.0032$) when Crp^{F46} was knocked down in HeLa cells. Based on these data, we discovered that the vast majority of changes in myosin IIA phosphorylation level linked to the regulation of the formation of myosin filaments. Interestingly, fluorescence microscope images (Fig. 5E) showed that, in Crp^{F46}-knockdown cells, the myosin IIA filaments became dim and almost exhibited diffuse distribution. However, the lack of Crp^{F46} did not affect the formation of myosin IIB (Supplementary material Fig. S3). Additionally, with transient transfected p3×Flag-cmv-Crp^{F46} vector, the phenotype of myosin IIA were rescued in cells, labeled by anti-Flag antibody (Fig. 5F). Therefore, we inferred that the decrease in the activity of non-muscle myosin IIA was caused by failure in myosin filament formation, which was induced by the changes in phosphorylation level of NMHC and RLC, when Crp^{F46} was knocked down in HeLa cells.

4. Discussion

We previously demonstrated that HeLa cells that were stably transfected with an antisense-Crp^{F46}-pXJ41 vector exhibited abnormal phenotypes, such as multiple centrosomes [23]. However, the presence of extra centrosomes disturbs cell migration by inducing multiple scattered microtubule organizing centers [34,35]. It is known that Crp^{F46} localizes to the centrosomes via its coiled-coil domain and regulates centrosome duplication [23]. Meanwhile, other molecular signal related to cell migration, such as matrix metalloproteinase and Rho GTPase, changed in different degrees (data not shown). So, the exploration of relationship between Crp^{F46} and migration is imperative. Here we firstly noticed a phenomenon (Fig. 1 and Supplementary material Fig. S1) worthy of attention: with the characteristics of multiple centrosomes, Crp^{F46}-knockdown cells reduced velocity of cell migration; their arrangement of microtubules became disordered which was assessed by fractal dimension. Fractal dimension can provide a statistical index of complexity in cellular structures (microtubules organization) by comparing details in a fractal pattern. Moreover, related to this, microtubules extended from MOTC (gathering points of green fluorescence) in control cells; however, the focus of the microtubule nucleation center was undetectable in Crp^{F46}-knockdown HeLa cells (Supplementary material Fig. S1H). It can be deduced by these data that the function of centrosomes in organizing microtubules was disrupted with Crp^{F46} low-expression.

In our research, in whether U-2OS or HeLa cell lines, the centrosomes were randomly positioned in the moving Crp^{F46}-knockdown cells, contrary to the properly oriented centrosomes in the control cells, which also can be found in the rescued cells (Fig. 2A and C; Supplementary material Fig. S2A and B). The statistical analyses

(Fig. 2E and F; Supplementary material Fig. S2C and D) were also consistent with the observable phenotypes. A corollary of centrosome relocation is cell polarity. The polar positioning of the centrosome is so important that leads to the polarity of the microtubule system and directional vesicular transport [36–38]. Due to their inflexible tubular structures, the nucleus remains at the central area of the cell, while microtubules extend from the centrosome and grow away from the nucleus, not around the nucleus, toward the scratch during a wound-induced cell migration. Correspondingly, most centrosomes are specifically oriented between the nucleus and leading edge of migration (Fig. 2B). Another marker of cell polarization is the orientation of Golgi apparatus (GA) [39] which closely surrounds the centrosome [40] and becomes directed to the leading edge [41] to ensure the functions of vesicular transport, e.g., movement of signaling molecules and cellular migration-associated materials for cellular locomotion [42]. From the perspective of GA location (Fig. 2G-I; Supplementary material Fig. S2F and G), in U-2OS or HeLa cells, the cell polarity reduced when Crp^{F46} was knocked down. Otherwise, the cell polarity was recovered after increasing Crp^{F46} (Fig. 2H and I). Meanwhile, molecular biomarkers showed the reduced level of Cdc42 protein in Crp^{F46}-knockdown HeLa cells (Supplementary material Fig. S2H and I). Researches in the same field revealed that Par complex plays a key role in maintaining cell polarization [43]. In the complex system, scaffold protein Par6 recruits small GTPase Cdc42 and serves as a regulatory subunit of PKC ζ [44]. Hence, the reduction of cell polarity got validated at the biochemistry level. Additionally, accurate observation of single-cell migration (Fig. 2J and Supplementary material Fig. S2E) directly provided chaotic performances on the motion of Crp^{F46}-knockdown cells. Therefore, the Crp^{F46} depletion reduced the cell migration velocity due to reduction of cell polarization and induction of random centrosomal orientation.

We designed a Co-IP assay and focused on the target protein NMHC IIA which has been validated by a series of experiments (Fig. 3). As the subunit of NM II providing mechanical force for cellular processes, NMHC IIA participates in driving cell migration. The contractility of actin filaments is achieved through three molecular mechanisms of myosin II modulating system, namely, the affinity between NM II and filamentous actin, ATPase activity of the catalytic sites on the amino-terminal (head) region of NM II, and self-association into filaments at the carboxy-terminal (tail) domain of NM II [18]. All these functional activities are regulated by phosphorylation of NMHC and the associated RLC. There are several phosphorylation sites located at the head and tail regions of NMHC II, including Ser1803, Ser1916, and Ser1943. Several studies in the literature have shown that Ser1803 [45] and Ser1916 [46,47] phosphorylation inhibits the assembly of NM II into filaments [22]. However, phosphorylation of Ser1943 by CKII [48] blocks the interaction between NMHC and S100A4, a protein preventing myosin II filamentation. In this study, since independence on the protein levels of Crp^{F46} and NMHC IIA (Fig. 5A and B), coordination between Crp^{F46} and NMHC IIA were considered in the direction of phosphorylation level. The phosphorylation sites of NMHC IIA changed on phosphorylation level (Fig. 5C and D), which suggests that the activity of NM IIA was blocked because of inhibition of its assembly into filaments. It is very pleasing that the

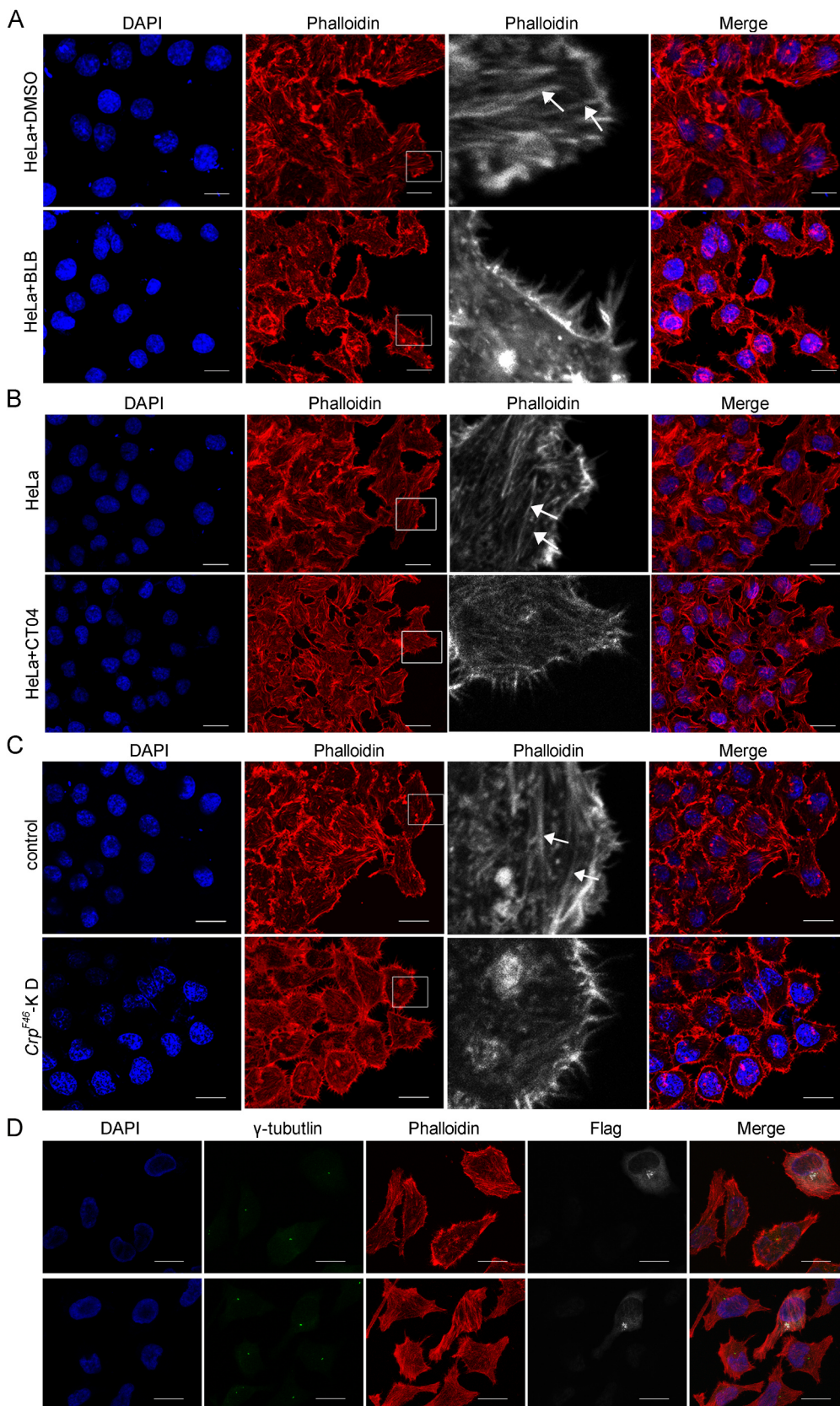


Fig. 4. Crp^{F46} functions the formation of the microfilament network regulated by NMHC IIA (A) Confocal microscopy images of F-actin stained with rhodamine-conjugated phalloidin in control cells and HeLa cells treated with 30 μ M blebbistatin. (B) Confocal microscope images of F-actin stained with a fluorescent phalloidin probe in control cells and HeLa cells treated with 5 μ M CT04. The white arrow denotes the stress fibers in binary image. The scale bars represent 20 μ m. (C) Confocal microscopy images of F-actin stained with rhodamine-conjugated phalloidin in control cells and Crp^{F46} -knockdown cells. (D) Confocal microscopy images of F-actin stained with rhodamine-conjugated phalloidin in Crp^{F46} -knockdown HeLa cells transiently transfected with recombinant p3×Flag-cmv- Crp^{F46} vectors. The white arrow denotes the stress fibers in binary image. The scale bars represent 20 μ m.

intuitive results, that NMHC IIA exhibited diffuse distribution in Crp^{F46} -knockdown cells, had been obtained from photomicrographs (Fig. 5E). But, the lack of Crp^{F46} in cells was not impacting the formation of myosin IIB filaments (Supplementary material Fig. S3). The rescued experiment

of myosin IIA filaments (Fig. 5F) also evidence that Crp^{F46} is necessary to maintain myosin IIA filaments. Apart from phosphorylation at the myosin heavy chain, phosphorylation at the NM II light chain has been implicated in determining the affinity to actin filaments and ATPase

activity [33]. Phosphorylation of Ser19 of RLC can increase actin affinity and ATPase activity and promote the walking of myosin along actin filaments [49,50]. Whereas protein kinase C (PKC)-mediated phosphorylation of Ser1, Ser2 and Thr9 on RLC allosterically renders Ser19 of RLC as a weaker poorer substrate for the kinase MLCK, thus decreasing the phosphorylation of Ser19 [51,52]. In addition, the PKC-catalyzed phosphorylation blocks the reorganization of actomyosin filaments [53]. Therefore, the increase in Ser1 phosphorylation and the decrease in of Ser19 phosphorylation on RLC as seen from our data (Fig. 5C and D) indicated the lack of NM II activity with down expression of *Crp^{F46}*. Unquestionably, the reduction of *Crp^{F46}* expression affects the activity of myosin.

Myosin II-driven contractility exerts tensile forces to promote directional migration of cells through stress fibers composed of bundles of approximately 10–30 actin filaments [54] and several actin-cross-linking proteins such as α -actinin [55] as well as myosin II itself [56]. To induce tension, myosin II hydrolyzes ATP on its head domain [18], walks along the filamentous actin and propels the sliding of actin filaments [57], which is necessary for the integrity of the stress fibers [58–61]. Additionally, Rho family small GTPases, especially RhoA, whose downstream effector is ROCK, regulate the activity of myosin II activity by phosphorylation [62] as was mentioned above. Consistently, the inhibitors of ROCK or myosin II can inhibit the formation of stress fibers [63–67]. Similarly, when the HeLa cells were treated with NM II inhibitor blebbistatin and Rho GTPase inhibitor CT04, the formation of stress fibers was greatly weakened, which were quantified with fractal dimension (Fig. 4A and B). Interestingly, the phenotype of weakened stress fibers assembly was also observed in the *Crp^{F46}*-deficient HeLa cells (Fig. 4C). However, the stress fibers became stronger after recovering Flag-*Crp^{F46}* into *Crp^{F46}*-knockdown cells (Fig. 4D), which proved *Crp^{F46}* played an important role in maintaining stress fibers. Hence, the similar phenotypic features among *Crp^{F46}*-knockdown cells and cells treated with blebbistatin or CT04, hinted the regulation of *Crp^{F46}* to NMHC IIA.

Combining results of the stress fibers phenotypes and the phosphorylation status of NM II, we can speculate that the inhibition of stress fibers in *Crp^{F46}*-knockdown cells occurred due to myosin inactivity. It has been discovered that in the response to extracellular and intracellular signals, ventral stress fibers provide tensile forces to contract the trailing area of directionally migration cells and dorsal stress fibers secure the extending pseudopod protrusion at the front [68], thereby establishing the front-to-back polarity axis, which is crucial for directional cell migration [20,69–71]. Furthermore, the forces generated by actomyosin cables run throughout the cytoplasm and drag the cell body [72]. Myosin II provides traction for relocation of centrosome [73]. If the activity of myosin or myosin kinases are inhibited, the relocation of centrosomes is irregular and the polarization of motile cells reduces [30,37,74]. Meanwhile, the lack of myosin phosphorylation, whether in NMHC or RLC, can disturb polarization of cells and migration velocity of cells [75,76]. These are probably deeper reasons why that knockdown of *Crp^{F46}* significantly distracted relocation of centrosomes and decreased the directional migration velocity of the tested cells. In conclusion, the intracellular shortage of *Crp^{F46}* blocks the formation of stress fibers, which contributes to the influence of centrosome reorientation and reduction of cellular locomotion ability, together with the deregulation of myosin activity stated above. In summary, this study verified that, as shown in Fig. 5G, *Crp^{F46}* is associated with NMHC IIA and regulates NM II activity via affecting phosphorylation, which is a crucial factor for the formation of stress fibers. Therefore, the deficiency of *Crp^{F46}* causes reduction of NM II activity resulting in weak stress fibers. On the other hand, the reorientation of centrosome is also disturbed by the drawback of NM II activity, which reduces consistency and directionality of microtubules arrangement and uncertainty of cellular polarization. All of abnormal phenotypes, including improper centrosomal reorientation, disorderly cellular polarization and weak stress fibers, give rise to delay of cell migration. In

conclusion, the actomyosin network is influenced by NMHC IIA and regulated by the factor *Crp^{F46}*, which is involved in the control of cell migration. This is a novel finding in the exploration of mechanisms involved in cellular movement and dynamic regulation of the cytoskeleton.

Acknowledgements

We thank Dr. Jian Kuang, Department of Experimental Therapeutics, University of Texas MD Anderson Cancer Center, for her constructive suggestions for the experimental design. We thank Prof. Junjie Zhang for providing the p3XFlag-cmv plasmid and Dr. Xiaoyan Zhang for her assistance with mass spectrometric analysis. We thank Dr. Jin Liu and senior experimentalist, An Peng, for their assistance with microphotography.

Funding

This work was supported by the National Natural Science Foundation of China (No. 31571394 to QL), the Beijing Natural Science Foundation (No. 5122017 to QL), the Open Fund of the Beijing Key Laboratory of Gene Resource and Molecular Development (No. 201504 to YZ), and the Open Fund of the Key Laboratory of Cell Proliferation and Regulation Biology, Ministry of Education of China (No. 201401 to YZ).

Conflicts of interest

The authors declare no conflicts of interest.

Appendix A. Supplementary material

Supplementary data associated with this article can be found in the online version at doi:10.1016/j.yexcr.2018.10.004.

References

- [1] M. Bettencourt-Dias, D.M. Glover, Centrosome biogenesis and function: centrosomes brings new understanding, *Nat. Rev. Mol. Cell Biol.* 8 (2007) 451–463.
- [2] B. Raynaud-Messina, A. Merdes, gamma-tubulin complexes and microtubule organization, *Curr. Opin. Cell Biol.* 19 (2007) 24–30.
- [3] M.P. Koonce, R.A. Cloney, M.W. Berns, Laser irradiation of centrosomes in newt eosinophils: evidence of centriole role in motility, *J. Cell Biol.* 98 (1984) 1999–2010.
- [4] M. Maninova, Z. Klimova, J.T. Parsons, M.J. Weber, M.P. Lwanicki, T. Vomastek, The reorientation of cell nucleus promotes the establishment of front-rear polarity in migrating fibroblasts, *J. Mol. Biol.* 425 (2013) 2039–2055.
- [5] A.M.C. Yvon, J.W. Walker, B. Danowski, C. Fagerstrom, A. Khodjakov, P. Wadsworth, Centrosome reorientation in wound-edge cells is cell type specific, *Mol. Biol. Cell* 13 (2002) 1871–1880.
- [6] M.C. Montoya, D. Sancho, M. Vicente-Manzanares, F. Sanchez-Madrid, Cell adhesion and polarity during immune interactions, *Immunol. Rev.* 186 (2002) 68–82.
- [7] M. Ueda, R. Graf, H.K. MacWilliams, M. Schliwa, U. Euteneuer, Centrosome positioning and directionality of cell movements, *Proc. Natl. Acad. Sci. USA* 94 (1997) 9674–9678.
- [8] A. Kupfer, D. Louvard, S.J. Singer, Polarization of the golgi-apparatus and the microtubule-organizing center in cultured fibroblasts at the edge of an experimental wound, *Proc. Natl. Acad. Sci.-Biol.* 79 (1982) 2603–2607.
- [9] A.I. Gotlieb, L.M. May, L. Subrahmanyam, V.I. Kalnins, Distribution of microtubule organizing centers in migrating sheets of endothelial-cells, *J. Cell Biol.* 91 (1981) 589–594.
- [10] L. Andres-Delgado, O.M. Anton, M.A. Alonso, Centrosome polarization in T cells: a task for formins, *Front. Immunol.* 4 (2013).
- [11] N.B. Martin-Cofreces, J. Robles-Valero, J.R. Cabrero, M. Mittelbrunn, M. Gordon-Alonso, C.H. Sung, B. Alarcon, J. Vazquez, F. Sanchez-Madrid, MTOC translocation modulates IS formation and controls sustained T cell signaling, *J. Cell Biol.* 182 (2008) 951–962.
- [12] D.J. Solecki, L. Model, J. Gaetz, T.M. Kapoor, M.E. Hatten, Par6 alpha signaling controls glial-guided neuronal migration, *Nat. Neurosci.* 7 (2004) 1195–1203.
- [13] D.J. Solecki, N. Trivedi, E.E. Govek, R.A. Kerekes, S.S. Gleason, M.E. Hatten, Myosin II motors and F-actin dynamics drive the coordinated movement of the centrosome and soma during CNS glial-guided, *Neuron. Migr. Neuron* 63 (2009) 63–80.
- [14] S. Even-Ram, A.D. Doyle, M.A. Conti, K. Matsumoto, R.S. Adelstein, K.M. Yamada, Myosin IIA regulates cell motility and actomyosin microtubule crosstalk, *Nat. Cell Biol.* 9 (2007) (299-U104).
- [15] M.A. Conti, R.S. Adelstein, Nonmuscle myosin II moves in new directions (vol 121,

- pg 11, 2008), *J. Cell Sci.* 121 (2008) (404–404).
- [16] A.F. Straight, A. Cheung, J. Limouze, I. Chen, N.J. Westwood, J.R. Sellers, T.J. Mitchison, Dissecting temporal and spatial control of cytokinesis with a myosin II inhibitor, *Science* 299 (2003) 1743–1747.
- [17] N. Billington, A.B. Wang, J. Mao, R.S. Adelstein, J.R. Sellers, Characterization of three full-length human nonmuscle myosin II paralogs, *J. Biol. Chem.* 288 (2013) 33398–33410.
- [18] M. Vicente-Manzanares, X.F. Ma, R.S. Adelstein, A.R. Horwitz, Non-muscle myosin II takes centre stage in cell adhesion and migration, *Nat. Rev. Mol. Cell Biol.* 10 (2009) 778–790.
- [19] J.D. Franke, R.A. Montague, W.L. Rickoll, D.P. Kiehart, An MYH9 human disease model in flies: site-directed mutagenesis of the *Drosophila* non-muscle myosin II results in hypomorphic alleles with dominant character, *Hum. Mol. Genet.* 16 (2007) 3160–3173.
- [20] C.M. Lo, D.B. Buxton, G.C.H. Chua, M. Dembo, R.S. Adelstein, Y.L. Wang, Nonmuscle myosin IIB is involved in the guidance of fibroblast migration, *Mol. Biol. Cell* 15 (2004) 982–989.
- [21] M. Ikebe, D.J. Hartshorne, M. Elzinga, Identification, phosphorylation, and dephosphorylation of a second site for myosin light chain kinase on the 20,000-dalton light chain of smooth muscle myosin, *J. Biol. Chem.* 261 (1986) 36–39.
- [22] N.G. Dulyaninova, V.N. Malashkevich, S.C. Almo, A.R. Bresnick, Regulation of myosin-IIA assembly and Mts1 binding by heavy chain phosphorylation, *Biochemistry* 44 (2005) 6867–6876.
- [23] Y. Wei, E.Z. Shen, N. Zhao, Q. Liu, J.L. Fan, J. Marc, Y.C. Wang, L. Sun, Q.J. Liang, Identification of a novel centrosomal protein Crp(F46) involved in cell cycle progression and mitosis, *Exp. Cell Res.* 314 (2008) 1693–1707.
- [24] T.G. Smith, G.D. Lange, W.B. Marks, Fractal methods and results in cellular morphology - dimensions, lacunarity and multifractals, *J. Neurosci. Methods* 69 (1996) 123–136.
- [25] V. Zinchuk, O. Grossenbacher-Zinchuk, Recent advances in quantitative colocalization analysis: focus on neuroscience, *Prog. Histochem. Cytochem.* 44 (2009) 125–172.
- [26] F. Bernard, J.L. Bossu, S. Gaillard, Identification of living oligodendrocyte developmental stages by fractal analysis of cell morphology, *J. Neurosci. Res.* 65 (2001) 439–445.
- [27] G.W.G. Luxton, G.G. Gundersen, Orientation and function of the nuclear-centrosomal axis during cell migration, *Curr. Opin. Cell Biol.* 23 (2011) 579–588.
- [28] S. Etienne-Manneville, Cdc42 - the centre of polarity, *J. Cell Sci.* 117 (2004) 1291–1300.
- [29] H. Daub, K. Gevaert, J. Vandekerckhove, A. Sobel, A. Hall, Rac/Cdc42 and p65PAK regulate the microtubule-destabilizing protein stathmin through phosphorylation at serine 16, *J. Biol. Chem.* 276 (2001) 1677–1680.
- [30] S. Etienne-Manneville, A. Hall, Integrin-mediated activation of Cdc42 controls cell polarity in migrating astrocytes through PKC zeta, *Cell* 106 (2001) 489–498.
- [31] E. Tzima, W.B. Kiosses, M.A. del Pozo, M.A. Schwartz, Localized Cdc42 activation, detected using a novel assay, mediates microtubule organizing center positioning in endothelial cells in response to fluid shear stress, *J. Biol. Chem.* 278 (2003) 31020–31023.
- [32] B. Honer, S. Giti, J. Kendrickjones, B.M. Jockusch, Modulation of cellular morphology and locomotory activity by antibodies against myosin, *J. Cell Biol.* 107 (1988) 2181–2189.
- [33] S.M. Heissler, J.R. Sellers, Various themes of myosin regulation, *J. Mol. Biol.* 428 (2016) 1927–1946.
- [34] Y. Mimori-Kiyosue, S. Tsukita, "Search-and-capture" of microtubules through plus-end-binding proteins (+TIPs), *J. Biochem.* 134 (2003) 321–326.
- [35] S.C. Schuyler, D. Pellman, Search, capture and signal: games microtubules and centrosomes play, *J. Cell Sci.* 114 (2001) 247–255.
- [36] E. Gomes, S. Jani, G. Gundersen, Nuclear movement regulated by Cdc42, MRCK, myosin and actin flow establishes MTOC polarization in migrating cells, *Cell Struct. Funct.* 30 (2005) (60–60).
- [37] A.F. Palazzo, H.L. Joseph, Y.J. Chen, D.L. Dujardin, A.S. Alberts, K.K. Pfister, R.B. Vallee, G.G. Gundersen, Cdc42 dynein, and dynactin regulate MTOC reorientation independent of Rho-regulated microtubule stabilization, *Curr. Biol.* 11 (2001) 1536–1541.
- [38] A.J. Ridley, M.A. Schwartz, K. Burridge, R.A. Firtel, M.H. Ginsberg, G. Borisy, J.T. Parsons, A.R. Horwitz, Cell migration: integrating signals from front to back, *Science* 302 (2003) 1704–1709.
- [39] N.L. Prigozhina, C.M. Waterman-Storer, Protein kinase D-mediated anterograde membrane trafficking is required for fibroblast motility, *Curr. Biol.* 14 (2004) 88–98.
- [40] R.M. Rios, The centrosome-Golgi apparatus nexus, *Philos. Trans. R. Soc. B* 369 (2014).
- [41] J. Schmoranz, G. Kreitzer, S.M. Simon, Migrating fibroblasts perform polarized, microtubule-dependent exocytosis towards the leading edge, *J. Cell Sci.* 116 (2003) 4513–4519.
- [42] T. Mazel, Crosstalk of cell polarity signaling pathways, *Protoplasma* 254 (2017) 1241–1258.
- [43] R. Insolera, S. Chen, S.H. Shi, Par proteins and neuronal polarity, *Dev. Neurobiol.* 71 (2011) 483–494.
- [44] L.M. McCaffrey, I.G. Macara, Signaling pathways in cell polarity, *Csh Perspect. Biol.* 4 (2012).
- [45] K. Clark, J. Middelbeek, E. Lasonder, N.G. Dulyaninova, N.A. Morrice, A.G. Ryzanov, A.R. Bresnick, C.G. Figdor, F.N. van Leeuwen, TRPM7 regulates myosin IIA filament stability and protein localization by heavy chain phosphorylation, *J. Mol. Biol.* 378 (2008) 790–803.
- [46] M.A. Conti, J.R. Sellers, R.S. Adelstein, M. Elzinga, Identification of the serine residue phosphorylated by protein-kinase-C in vertebrate nonmuscle myosin heavy-chains, *Biochemistry* 30 (1991) 966–970.
- [47] R.I. Ludowyke, Z. Elgundi, T. Kranenburg, J.R. Stehn, C. Schmitz-Peiffer, W.E. Hughes, T.J. Biden, Phosphorylation of nonmuscle myosin heavy chain IIA on Ser1917 is mediated by protein kinase C beta II and coincides with the onset of stimulated degranulation of RBL-2H3 mast cells, *J. Immunol.* 177 (2006) 1492–1499.
- [48] Z.H. Li, A.R. Bresnick, The S100A4 metastasis factor regulates cellular motility via a direct interaction with myosin-IIA, *Cancer Res.* 66 (2006) 5173–5180.
- [49] J.M. Scholey, K.A. Taylor, J. Kendrickjones, Regulation of non-muscle myosin assembly by calmodulin-dependent light chain kinase, *Nature* 287 (1980) 233–235.
- [50] K.M. Trybus, Filamentous smooth-muscle myosin is regulated by phosphorylation, *J. Cell Biol.* 109 (1989) 2887–2894.
- [51] S. Umemoto, A.R. Bengur, J.R. Sellers, Effect of multiple phosphorylations of smooth muscle and cytoplasmic myosins on movement in an in vitro motility assay, *J. Biol. Chem.* 264 (1989) 1431–1436.
- [52] N.S. Bryce, G. Schevzov, V. Ferguson, J.M. Percival, J.J. Lin, F. Matsumura, J.R. Bamburg, P.L. Jeffrey, E.C. Hardeman, P. Gunning, R.P. Weinberger, Specification of actin filament function and molecular composition by tropomyosin isoforms, *Mol. Biol. Cell* 14 (2003) 1002–1016.
- [53] S. Komatsu, M. Ikebe, The phosphorylation of myosin II at the Ser1 and Ser2 is critical for normal platelet-derived growth factor-induced reorganization of myosin filaments, *Mol. Biol. Cell* 18 (2007) 5081–5090.
- [54] L.P. Cramer, M. Siebert, T.J. Mitchison, Identification of novel graded polarity actin filament bundles in locomoting heart fibroblasts: implications for the generation of motile force, *J. Cell Biol.* 136 (1997) 1287–1305.
- [55] E. Lazarides, K. Burridge, Alpha-actinin - immunofluorescent localization of a muscle structural protein in nonmuscle cells, *Cell* 6 (1975) 289–298.
- [56] S. Lee, S. Kumar, Actomyosin stress fiber mechanosensing in 2D and 3D, *F1000Research* 5 (2016).
- [57] Q. Chi, T. Yin, H. Gregersen, X. Deng, Y. Fan, J. Zhao, D. Liao, G. Wang, Rear actomyosin contractility-driven directional cell migration in three-dimensional matrices: a mechano-chemical coupling mechanism, *J. R. Soc. Interface* 11 (2014) 20131072.
- [58] M. Chrzanoska-Wodnicka, K. Burridge, Rho-stimulated contractility drives the formation of stress fibers and focal adhesions, *J. Cell Biol.* 133 (1996) 1403–1415.
- [59] J. Bao, S.S. Jana, R.S. Adelstein, Vertebrate nonmuscle myosin II isoforms rescue small interfering RNA-induced defects in COS-7 cell cytokinesis, *J. Biol. Chem.* 280 (2005) 19594–19599.
- [60] P. Hotulainen, P. Lappalainen, Stress fibers are generated by two distinct actin assembly mechanisms in motile cells, *J. Cell Biol.* 173 (2006) 383–394.
- [61] J. Kolega, The role of myosin II motor activity in distributing myosin asymmetrically and coupling protrusive activity to cell translocation, *Mol. Biol. Cell* 17 (2006) 4435–4445.
- [62] P. Naumanen, P. Lappalainen, P. Hotulainen, Mechanisms of actin stress fibre assembly, *J. Microsc.-Oxf.* 231 (2008) 446–454.
- [63] M. Uehata, T. Ishizaki, H. Satoh, T. Ono, T. Kawahara, T. Morishita, H. Tamakawa, K. Yamagami, J. Inui, M. Maekawa, S. Narumiya, Calcium sensitization of smooth muscle mediated by a Rho-associated protein kinase in hypertension, *Nature* 389 (1997) 990–994.
- [64] B. Kovac, J.L. Teo, T.P. Makela, T. Vallenius, Assembly of non-contractile dorsal stress fibers requires alpha-actinin-1 and Rac1 in migrating and spreading cells, *J. Cell Sci.* 126 (2013) 263–273.
- [65] J.C. Kuo, X.M. Han, C.T. Hsiao, J.R. Yates, C.M. Waterman, Analysis of the myosin-II-responsive focal adhesion proteome reveals a role for beta-Pix in negative regulation of focal adhesion maturation, *Nat. Cell Biol.* 13 (2011) (383-U109).
- [66] A.M. Pasapera, I.C. Schneider, E. Rericha, D.D. Schlaepfer, C.M. Waterman, Myosin II activity regulates vinculin recruitment to focal adhesions through FAK-mediated paxillin phosphorylation, *J. Cell Biol.* 188 (2010) 877–890.
- [67] H.B. Schiller, C.C. Friedel, C. Bouleue, R. Fassler, Quantitative proteomics of the integrin adhesomes show a myosin II-dependent recruitment of LIM domain proteins, *Embo Rep.* 12 (2011) 259–266.
- [68] S. Pellegrin, H. Mellor, Actin stress fibres, *J. Cell Sci.* 120 (2007) 3491–3499.
- [69] S.F. Ang, Z.S. Zhao, L. Lim, E. Manser, DAAM1 is a formin required for centrosome re-orientation during cell migration, *PLoS One* 5 (2010).
- [70] M. Vicente-Manzanares, M.A. Koach, L. Whitmore, M.L. Lamers, A.F. Horwitz, Segregation and activation of myosin IIB creates a rear in migrating cells, *J. Cell Biol.* 183 (2008) 543–554.
- [71] M. Vicente-Manzanares, K. Newell-Litwa, A.I. Bachir, L.A. Whitmore, A.R. Horwitz, Myosin IIA/IIB restrict adhesive and protrusive signaling to generate front-back polarity in migrating cells, *J. Cell Biol.* 193 (2011) 381–396.
- [72] S. Etienne-Manneville, Microtubules in cell migration, *Annu. Rev. Cell Dev. Biol.* 29 (2013) 471–499.
- [73] J. Elic, S. Etienne-Manneville, Centrosome positioning in polarized cells: common themes and variations, *Exp. Cell Res.* 328 (2014) 240–248.
- [74] J.B. Manneville, M. Jehanno, S. Etienne-Manneville, Dlg1 binds GKAP to control dynein association with microtubules, centrosome positioning, and cell polarity, *J. Cell Biol.* 191 (2010) 585–598.
- [75] J.H. Lee, H. Koh, M. Kim, Y. Kim, S.Y. Lee, R.E. Kares, S.H. Lee, M. Shong, J.M. Kim, J. Kim, J. Chung, Energy-dependent regulation of cell structure by AMP-activated protein kinase, *Nature* 447 (2007) 1011–1020.
- [76] H.M. Phillips, J.N. Murdoch, B. Chaudhry, A.J. Copp, D.J. Henderson, Vangl2 acts via RhoA signaling to regulate polarized cell movements during development of the proximal outflow tract, *Circ. Res.* 96 (2005) 292–299.